CHIN. PHYS. LETT. Vol. 38, No. 12 (2021) 127201

Realizing n-Type GeTe through Suppressing the Formation of Cation Vacancies and Bi-Doping

Min Zhang(张敏), Chaoliang Hu(胡超亮), Qi Zhang(张奇), Feng Liu(刘锋), Shen Han(韩屾), Chenguang Fu(付晨光), and Tiejun Zhu(朱铁军)*

School of Materials Science and Engineering, and State Key Laboratory of Silicon Materials, Zhejiang University, Zhejiang 310027, China

(Received 28 August 2021; accepted 28 October 2021; published online 18 November 2021)

It is known that p-type GeTe-based materials show excellent thermoelectric performance due to the favorable electronic band structure. However, n-type doping in GeTe is of challenge owing to the native Ge vacancies and high hole concentration of about $10^{21}\,\mathrm{cm}^{-3}$. In the present work, the formation energy of cation vacancies of GeTe is increased through alloying PbSe, and further Bi-doping enables the change of carrier conduction from p-type to n-type. As a result, the n-type thermoelectric performance is obtained in GeTe-based materials. A peak zT of 0.34 at 525 K is obtained for $(Ge_{0.6}Pb_{0.4})_{0.88}Bi_{0.12}Te_{0.6}Se_{0.4}$. These results highlight the realization of n-type doping in GeTe and pave the way for further optimization of the thermoelectric performance of n-type GeTe.

DOI: 10.1088/0256-307X/38/12/127201

Most of the energy in industrial production is dissipated into the atmosphere in the form of waste heat.[1] Thermoelectric technology can directly convert heat into electricity and has received extensive renewed attention.[2,3] The performance of thermoelectric materials is gauged by the dimensionless thermoelectric figure-of-merit zT, $zT = S^2\sigma T/(\kappa_\mathrm{l} + \kappa_\mathrm{e})$, where S is the Seebeck coefficient, σ is the electrical conductivity, T is the absolute temperature, κ_l and κ_e are the thermal conductivity contributed by phonons and electrons respectively.[4,5] The thermoelectric performance of a material is determined by the synergistic effect of its electrical and thermal properties.[6]

A large number of compound semiconductor materials were found to show promising thermoelectric performance in the medium of the last century attributed to the development of the band theory. Till now, many efforts have been devoted to the Bi_2Te_3[7] for near-room-temperature refrigeration and half-Heusler,[8] skutterudites,[9] group IV–VI chalcogenides[10] for power generation at elevated temperatures. The semiconducting group IV–VI chalcogenides, especially GeTe, SnTe, and PbTe, show excellent thermoelectric performance in the mid-temperature range (500–800 K).[11,12] Compared with PbTe, the toxic-elements-free GeTe-based thermoelectric materials are environmentally friendly. Also, GeTe shows a higher thermoelectric performance than that of SnTe because of the favorable band structure.[13] Since the 1960s when GeTe-based materials were known as promising thermoelectrics,[14] the achievable zT of p-type GeTe has broken records multiple times.[15,16] A record zT of 2.5 was recently realized in GeTe-Cu_2Te-PbSe alloy, which is one of the highest zT values reported so far.[17]

The superior electrical properties of p-type GeTe-based thermoelectric materials mainly benefit from the favorable band structure. The valence bands devoted to hole conduction mainly contain the heavy Σ and light L bands with band degeneracies of 12 and 4, respectively.[13] GeTe alone behaves as a heavily doped p-type semiconductor owing to the thermodynamically driven cation (Ge) vacancies. The native hole density in undoped GeTe is up to $8\times10^{20}\,\mathrm{cm}^{-3}$,[18–20] much higher than the optimal carrier density ($2\times10^{20}\,\mathrm{cm}^{-3}$ at 670 K). Most of the previous studies on p-type GeTe mainly focused on reducing the carrier concentration and enabling band convergence to optimize the electrical properties. The hole density can be effectively reduced through compensatory doping at the cation site, such as Bi[10,21] and Sb.[22,23] Li *et al.* also found that alloying GeTe with PbSe increases the formation energy of Ge vacancies, thereby inhibiting the formation of Ge vacancies and reducing the hole concentration.[24] On the other hand, doping with divalent elements such as Mn,[25] Cd,[26] and Zn[27] was reported to be effective in narrowing the gap between the two valence bands, which might enable the realization of band convergence. The influence of magnetism[28] on thermoelectric performance is also studied in Mn-doped GeTe alloy.[29] Moreover, multi-element co-doping is a common method for im-

Supported by the National Science Fund for Distinguished Young Scholars (Grant No. 51725102), and the National Natural Science Foundation of China (Grant No. 51861145305).
*Corresponding author. Email: zhutj@zju.edu.cn
© 2021 Chinese Physical Society and IOP Publishing Ltd

proving the thermoelectric performance.[30]

In addition to the electrical properties, the thermal conductivity also plays a vital role in the figure-of-merit zT. The presence of the lone pair s-electrons of divalent group-IV elements leads to a large anharmonicity.[31] The unique bonding structure of IV–VI group compounds leads to a relatively low intrinsic lattice thermal conductivity without sacrificing carrier mobility. Increasing the phonon scattering to further reduce the thermal conductivity is also a common means of performance optimization in GeTe-based materials. Xu *et al.* introduced disc-shaped Ge vacancy clusters into the matrix through heat treatment, which is effective in scattering intermediate-frequency phonons, resulting in the reduction of lattice thermal conductivity.[32] The domain structure at the micron scale also plays a role in lowering thermal conductivity. During the cooling process from the liquid state, GeTe undergoes a phase transition from the high-temperature cubic to the low-temperature rhombohedral phase at about 720 K.[33] The crystal region with different rhombohedral axes forms a herringbone domain structure. It was supposed that the regularly arranged domain structure contributes to the low lattice thermal conductivity at room temperature because the domain boundaries can scatter long-wavelength phonons.[22,34] However, the structural instability is detrimental to long-term application, especially when the highest zT occurs near the transition temperature. Therefore, much effort has been made in lowering the transition temperature down to room temperature and below.[35,36]

In comparison to the extensive studies on p-type GeTe, there are few studies on the n-type GeTe. Askarpour *et al.* investigated the anisotropic thermoelectric transport in quasi-two-dimensional rhombohedral GeTe via *ab initial* calculation.[37] Surprisingly, unlike p-type GeTe, they found that n-type GeTe could have the higher carrier mobility along [111] direction, while the lattice thermal conductivity is smaller along this direction. They predicted that the highest zT of n-type GeTe can be even larger than that of p-type GeTe. Zachary *et al.* proposed a descriptor, i.e., Fermi surface complexity factor Nv^*K^*, to evaluate whether a material with a specific band structure has the potential to realize high thermoelectric performance.[38] As from their prediction, n-type GeTe has the largest Nv^*K^*, indicating that it could exhibit good thermoelectric performance. However, these predictions have not yet been validated because of the rare experimental studies on n-type GeTe. Manisha *et al.* realized n-type doping in GeTe-based materials via alloying with $AgBiSe_2$.[39] When the alloying content of $AgBiSe_2$ is higher than 30%, the alloys exhibit n-type semiconducting behavior. Liu *et al.* fabricated n-type GeTe by heavily doping of Bi as well as alloying with $AgInTe_2$.[40] To date, all the reported n-type TE performance in GeTe is greatly inferior to the p-type. The obtained maximum n-type zT is ∼0.6 in $(GeTe)_{50}(AgBiSe_{1.995}Br_{0.005})_{50}$ at 500 K.[37] However, introducing such a large amount of $AgBiSe_2$ into GeTe remarkably changes the favorable band structure of GeTe due to the increased contribution of Bi p orbitals in the conduction band edge, and the inevitable precipitates Ag_2Te may deteriorate the thermal stability.

As mentioned above, it is the native high-concentration Ge vacancies in GeTe that make it exhibit a strong p-type degenerate semiconductor behavior. To realize n-type doping in GeTe, we think that two steps are necessary: (1) inhibiting the formation of Ge vacancies through increasing the vacancy formation energy, (2) doping with elements that can provide additional electrons, such as group-V element Bi on Ge site. PbSe is thermally stable and its band structure is similar to that of GeTe.[41] Here, the vacancy formation energy of GeTe is increased by alloying with PbSe. With further Bi-doping, n-type GeTe-based materials are successfully realized. Because of a large amount of PbSe introduced into the GeTe-based alloys, the thermal conductivity is significantly suppressed, which is close to the amorphous limit ($0.41\ W{\cdot}m^{-1}{\cdot}K^{-1}$) near room temperature. Eventually, with 12% Bi doping, a peak zT of 0.34 is obtained at 525 K for $(Ge_{0.6}Pb_{0.4})_{0.88}Bi_{0.12}Te_{0.6}Se_{0.4}$.

Experiment. High pure raw materials Ge (99.99%), Te (99.999%), Pb (99.99%), Se (99.99%), and Bi (99.999%) were sealed in a vacuum quartz tube with stoichiometric ratio of $(Ge_{0.6}Pb_{0.4})_{1-x}Bi_xTe_{0.6}Se_{0.4}$ (x = 0, 0.05, 0.08, 0.10, 0.12, 0.15), then melted at 1223 K for 10 h and annealed at 773 K for 24 h. After that, the well-crystalline ingots were grounded manually into powders (∼50 μm in diameters) in air, and then pressed into the pellets of 12.7 mm in diameters and 2 mm in thickness by hot-pressing at 853 K for 40 min under a uniaxial pressure of 79 MPa (4505 J, MRF). For the convenience of description, the abbreviation GPTS-x is used below, where x is the nominal concentration of Bi.

The powder x-ray diffractions (PXRD) were recorded using a Cu K_α (λ = 1.5406 Å) radiation (Aries, DY866). A scanning electron microscope (SEM, SU-8010) was utilized to observe the polished surfaces of samples and an electron probe microanalyzer (EPMA, JEOL JXA-8100) with a wavelength dispersive spectroscope was used to analyze element distribution. The thermal diffusivity (D) was measured by a Netzsch LFA467 laser flash system. The thermal conductivity was determined via $\kappa = DC_Pd$, where a Dulong–Petit limit of heat capacity (C_P) was used, and the density (d) was determined by the Archimedes method. The Seebeck coefficient S and

resistivity ρ were simultaneously measured by a commercial Linseis LSR-3 system.

The formation energy of Ge anti-site (Ge_{Te}), Te anti-site (Te_{Ge}), Te vacancy (V_{Te}), and Ge vacancy (V_{Ge}) was determined according to[42]

$$E_f[X] = E_{tot}[X] - E_{tot}[\text{GeTe, bulk}] - \sum_i n_i \mu_i,$$

where the total energy of a defective and a perfect supercell was calculated based on the density functional theory, using the Vienna *ab initio* simulation package.[43] The Perdew–Burke–Ernzerhof type generalized gradient approximation[44] was applied as the exchange correlation functional. A plane-wave energy cutoff of 400 eV and an energy convergence criterion of 10^{-5} eV for self-consistency were adopted. We adopted $4 \times 4 \times 4$ supercells containing 128 atoms of GeTe alloyed with different concentrations of PbSe. One point defect was introduced in the quasi-random supercell to calculate the formation energy. The chemical potential part was determined by assuming a Ge-rich environment.

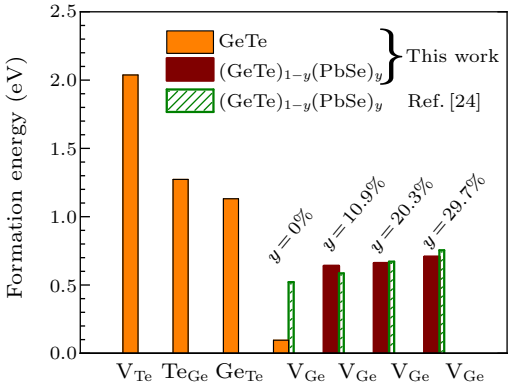

Fig. 1. The calculated formation energy of several types of point defects in GeTe (orange) and that of Ge vacancy in $(GeTe)_{1-y}(PbSe)_y$ alloy with y equal to 10.9%, 20.3%, and 29.7% (wine). The calculated results by Li *et al.*[24] are also presented here for comparison (green).

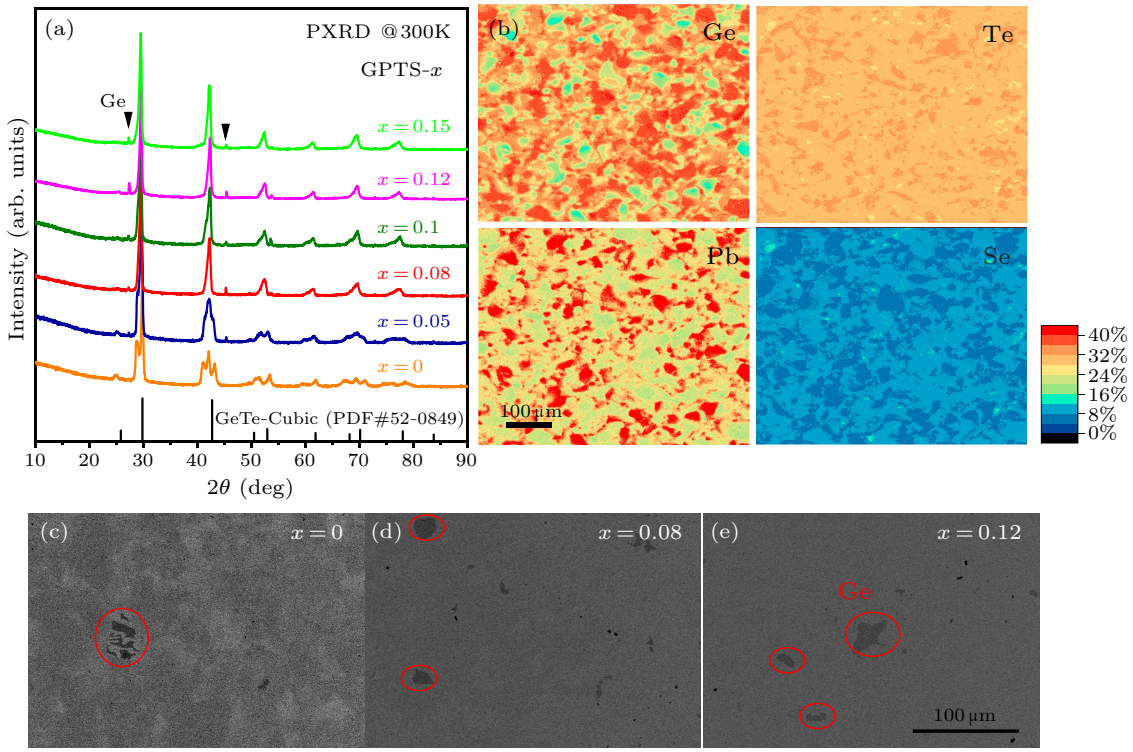

Fig. 2. (a) Powder x-ray diffraction patterns of $(Ge_{0.6}Pb_{0.4})_{1-x}Bi_xTe_{0.6}Se_{0.4}$ (x = 0, 0.05, 0.08, 0.1, 0.12, 0.15), (b) elemental distribution map of $(GeTe)_{0.6}(PbSe)_{0.4}$ alloy, (c)–(e) backscattered electron images of the polished surfaces.

Results and Discussion. The formation energy of several types of point defects in GeTe was calculated, and the results are shown in Fig. 1. Among them, Ge vacancy has the much lower formation energy compared to other possible point defects. As a result, Ge vacancies are the dominant point defects in GeTe. The formation energy of Ge vacancy for GeTe calculated in this work is lower than that by Li *et al.*[24] It is attributed to the difference in the size of the supercell, and the results in this work are more in line with those in other reports.[15,45] It is also seen from Fig. 1 that alloying with PbSe leads to an increase in the formation energy of Ge vacancies. Therefore, in this work, PbSe-alloying is chosen to reduce the Ge vacancies in GeTe. Considering the solid-solution limit of PbSe in GeTe,[24] the ratio of GeTe to PbSe is set to be 6 : 4,

i.e., the matrix $(GeTe)_{0.6}(PbSe)_{0.4}$(GPTS) is selected.

As shown in Fig. 2(a), room-temperature PXRD of GPTS-x could be indexed to the cubic structure (space group 225), indicating that PbSe alloying and Bi-doping enable the shift of the phase transition temperature down to below room temperature. The extra diffraction peak at 27° indicates the presence of germanium, which is commonly observed in the synthesized GeTe-based materials. It is worth noting that the main peak at 29° of the sample GPTS-0 splits, indicating that the solubility of Pb or Se in GeTe is likely to be less than 40%, inconsistently with the previous reports.[24] The elemental distribution map of the GPTS-0 sample shows the non-uniform distribution of the elements, especially Ge and Pb, as shown in Fig. 2(b). The image of backscattered electrons (BSE) [Figs. 2(c)–2(e)] shows that the contrast in the matrix disappears as the Bi content increases, suggesting that doping with Bi can effectively enhance the solubility of Pb and Se in GeTe. It is worth noting that, as the concentration of Bi increases, the contents of secondary phase Ge (dark spots) increase, which is also evident in the PXRD patterns showing an obvious Ge diffraction peak in the sample GPTS-x [Fig. 2(a)]. This qualitatively demonstrates that the increase of Bi element promotes the formation of Ge vacancies, agreeing with the previous report.[26]

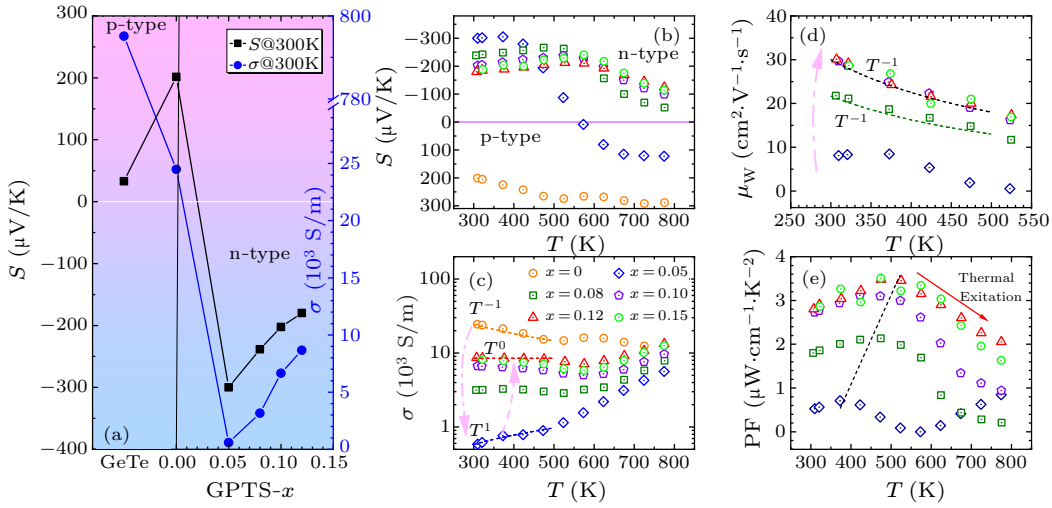

Fig. 3. (a) Electrical properties of GeTe and GPTS-x at 300 K; temperature-dependent Seebeck coefficient (b), electrical conductivity (c), weighted mobility (d), and power factor (e) of GPTS-x. The dotted lines are guiding lines to the temperature dependence [(c), (d)] or the thermal excitation temperature (e).

The electrical properties of GPTS-x are shown in Fig. 3. It can be seen from Fig. 3(a) that the electrical conductivity at room temperature is greatly reduced, and the Seebeck coefficient increases after alloying with PbSe, suggesting the reduced hole concentration and the suppressed formation of cation vacancies. Further doping with Bi at cation sites changes the carrier conduction from p-type to n-type, and the electrical conductivity increases as Bi content increases. It is worth noting that merely doping with Bi to provide electrons can hardly turn p-type GeTe to n-type because the density of intrinsic cation vacancy is very high and the formation energy of Ge vacancy decreases as E_F moves towards the conduction band.[40] In this work, GeTe is alloyed with PbSe to suppress the formation of cation vacancies, which makes it possible to achieve n-type conduction with further Bi-doping.

The temperature-dependent Seebeck coefficient (S) in Fig. 3(b) clearly shows the transition from p-type to n-type as the Bi content increases. However, as temperature increases, the Seebeck coefficient of GPTS-0.05 changes back from n-type to p-type. There may be two reasons for this transition: first, holes contribute more to the electrical conductivity even if electrons and holes increase simultaneously at high temperature, which may result from the higher mobility of holes than that of electrons; second, as temperature increases, the concentration of Ge vacancies increases, generating more holes. Other dopants such as Cu_2Te,[46,47] CuSb,[48] and Sb_2Te_3[49] have similar effects on increasing the formation energy of Ge-vacancy as PbSe-alloying. However, introducing these dopants are not enough to bring about the transition of the conduction type. The formation energy of Ge-vacancy decreases significantly when E_F moves towards the conduction band.[40] As a result, alloying with PbSe is a feasible strategy to realize n-type GeTe via Ge vacancies suppression.

The electrical conductivity of $(GeTe)_{0.6}(PbSe)_{0.4}$ alloy first dramatically decreases and then increases with increasing Bi contents [the trend is shown by the pink arrow in Fig. 3(c)], indicating the rising

electron concentration. However, compared with p-type GeTe alloys, the electrical conductivity of n-type GeTe alloys is much lower by more than one order of magnitude, which results from the complex element composition and the large concentration of dopants. The electrical conductivity of GPTS-x with x higher than 8% changes nearly temperature-independently below 600 K, which indicates a mixed carrier scattering mechanism.

Due to the complicated transport mechanism of the complex system with multiple elements coexisting in this work, it is difficult to obtain reliable carrier concentration data from the Hall resistivity measurements. In this case, the weighted mobility ($\mu_{\rm w}$) which is estimated by the Seebeck coefficient and electrical conductivity is applicable for analyzing the transport properties.[50] The temperature-dependent $\mu_{\rm w}$ of n-type GPTS-x alloy is shown in Fig. 2(d), which intuitively reflects the transport properties of the sample. When acoustic phonon scattering dominates, the weighted mobility decreases with temperature with a $T^{-3/2}$ dependence. Thus the T^{-1} dependence in this work [Fig. 3(d)] indicates the existence of other scattering mechanisms. The $\mu_{\rm w}$ increases significantly as the concentration of dopant increases when x is lower than 0.1. It is speculated that the ionic impurity scattering may be the dominant scattering mechanism in GPTS-0.05 because of the extremely low electron concentration. As Bi content increases, the ionic impurity scattering is weakened because of the increased carrier concentration.[51] However, further doping with Bi does not help to increase the $\mu_{\rm w}$. This is because the $\mu_{\rm w}$ is independent of carrier concentration when the scattering mechanism and band structure are fixed.

The Seebeck coefficient decreases while the electrical conductivity rises rapidly above about 600 K, resulting from the intrinsic excitation. The band gap calculated by the Goldsmid–Sharp model[52] ($E_{\rm g} = 2S_{\max}T_{\max}$) is about 0.23 eV and is almost unchanged with increasing Bi content. As shown in Fig. 3(e), the peak power factor (PF $= S^2\sigma$) is improved and the intrinsic excitation setup temperature rises with increasing Bi content.

Although Bi-doping succeeds in increasing the electron concentration, its doping efficiency is relatively low and the electron concentration can hardly be further increased by increasing the concentration of dopant Bi. The low doping efficiency of Bi-doping is most likely due to the fact that Bi doping decreases the formation energy of Ge vacancy, as indicated by the PXRD patterns and the images of backscattered electrons in Fig. 2. As a result, the increased Ge vacancies impede the further optimization of the electron concentration.

Alloying with 40% PbTe dramatically reduces the thermal conductivity to an amorphous solid limit near room temperature, as illustrated in Fig. 4(a). The dotted line refers to the minimum lattice thermal conductivity at the amorphous solid limit using the Cahill model.[53] The speed of sound was measured for the $Ge_{0.6}Pb_{0.4}Te_{0.6}Se_{0.4}$ sample, in which the transverse ($v_{\rm t}$) and longitudinal acoustic velocities ($v_{\rm l}$) are 1614 m/s and 3016 m/s, respectively, corresponding to its low thermal conductivity. The electronic contribution $\kappa_{\rm e}$ to the thermal conductivity is estimated via $\kappa_{\rm e} = L\sigma T$, where the Lorentz number L is determined by the single parabolic band model with a given S at low temperature and fixed as $1.5 \times 10^{-8}\,{\rm V^2/K^2}$ above 500 K. The lattice thermal conductivity (short-dashed lines) is estimated by subtracting the electronic part. Due to the extremely low electrical conductivity, the thermal conductivity contributed by the charge carriers is negligible. As temperature increases, the thermal conductivity contributed by bipolar diffusion increases and dominates above 400 K. Compared with the reported $(GeTe)_{50}(AgBiSe_{1.995}Br_{0.005})_{50}$ by Manisha *et al.*,[39] the GPTS-0.12 in this work shows similar electrical properties, but a higher thermal conductivity. The extremely low thermal conductivity ($\sim$0.33 $\rm W{\cdot}m^{-1}{\cdot}K^{-1}$) of $(GeTe)_{50}(AgBiSe_{1.995}Br_{0.005})_{50}$ is attributed to the formation of domain structure and grain boundaries and the presence of Ge and Ag_2Te. However, the existence of the unstable precipitates Ag_2Te is detrimental to the thermal stability of the samples. Here, in our GPTS-x samples, the only precipitates are Ge, which is stable throughout the testing temperature range.

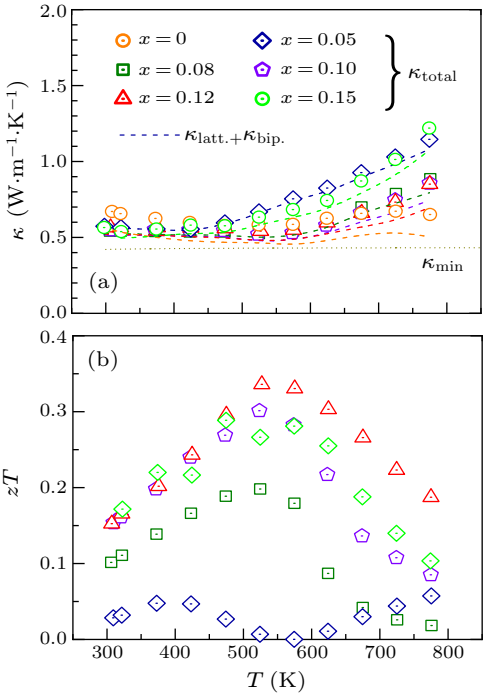

Fig. 4. (a) Thermal conductivity and (b) zT of the GPTS-x samples versus temperature.

The temperature-dependent figure-of-merit zT is shown in Fig. 4(b). Increasing the Bi content helps to optimize the zT during the whole testing temperature. However, the zT drops when the Bi content is higher than 12%. Due to the serious decline in the Seebeck coefficient and the large increase in thermal conductivity caused by the intrinsic activation, zT deteriorates severely at high temperatures. A peak zT of 0.34 is obtained for GPTS-0.12 at 525 K. To further optimize the thermoelectric performance of n-type GeTe alloys, one should focus on finding a more efficient way to improve the electron concentration and to suppress the formation energy of Ge vacancies.

In addition, the thermogravimetric analysis of GPTS-x was carried and the results are presented in Fig. 5. The weight loss above 750 K indicates slight volatilization, which is commonly found for selenides. Below 750 K, the samples keep thermally stable, indicating a safe working temperature range. Moreover, the Seebeck coefficient changes negligibly in the testing temperature range [Fig. 5(b)], which further proves the stability of the n-type GeTe alloy in this work.

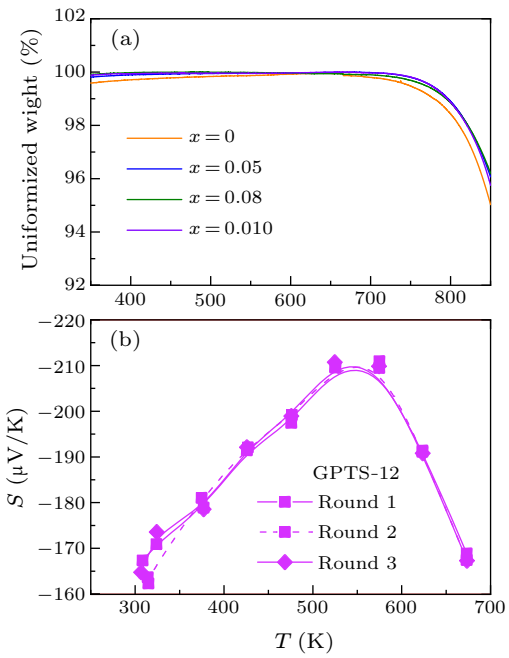

Fig. 5. (a) Thermogravimetric analysis (TGA) of GPTS-x and (b) repeatability test of GPTS-12.

In summary, we have successfully obtained n-type GeTe alloys by alloying with PbSe and Bi-doping. The former effectively increases the formation energy of cation vacancies and reduces the vacancy concentration, while the latter provides excess electrons, resulting in n-type conduction in the entire testing temperature range. Increasing the content of Bi can only promote the electron concentration to a certain extent. The complex elemental composition greatly reduces the thermal conductivity to the amorphous limit but also sacrifices the carrier mobility simultaneously. The analysis of the weighted mobility indicates that multiple scattering mechanisms coexist in the studied n-type GeTe alloys. A peak zT of 0.34 is obtained in GPTS-0.12 at 525 K. The studied samples show good thermal stability below 750 K.

References

[1] Bell L E 2008 *Science* **321** 1457
[2] Zebarjadi M, Esfarjani K, Dresselhaus M S, Ren Z F and Chen G 2012 *Energy Environ. Sci.* **5** 5147
[3] Snyder G J and Toberer E S 2008 *Nat. Mater.* **7** 105
[4] Goldsmid H J 2013 *Introduction to Thermoelectricity* (Berlin: Springer) p 3
[5] Zhu T, Liu Y, Fu C, Heremans J P, Snyder J G and Zhao X 2017 *Adv. Mater.* **29** 1605884
[6] Minnich A J, Dresselhaus M S, Ren Z F and Chen G 2009 *Energy Environ. Sci.* **2** 466
[7] Hao F, Qiu P, Tang Y, Bai S, Xing T, Chu H S, Zhang Q, Lu P, Zhang T, Ren D, Chen J, Shi X and Chen L 2016 *Energy Environ. Sci.* **9** 3120
[8] Zhu T, Fu C, Xie H, Liu Y and Zhao X 2015 *Adv. Energy Mater.* **5** 1500588
[9] Shi X, Yang J, Salvador J R, Chi M, Cho J Y, Wang H, Bai S, Yang J, Zhang W and Chen L 2011 *J. Am. Chem. Soc.* **133** 7837
[10] Li J, Zhang X, Chen Z, Lin S, Li W, Shen J, Witting I T, Faghaninia A, Chen Y, Jain A, Chen L, Snyder G J and Pei Y 2018 *Joule* **2** 976
[11] Roychowdhury S, Samanta M, Perumal S and Biswas K 2018 *Chem. Mater.* **30** 5799
[12] Ravich Y I 1970 Semiconducting Lead Chalcogenides (New York: Springer Science + Busness Media)
[13] Li J, Chen Z, Zhang X, Sun Y, Yang J and Pei Y 2017 *NPG Asia Mater.* **9** e353
[14] Rosi F D, Dismukes J P and Hockings E F 1960 *Electr. Eng.* **79** 450
[15] Zhang X, Bu Z, Lin S, Chen Z, Li W and Pei Y 2020 *Joule* **4** 986
[16] Hong M, Zou J and Chen Z G 2019 *Adv. Mater.* **31** 1807071
[17] Bu Z L, Zhang X Y, Shan B, Tang J, Liu H X, Chen Z W, Lin S q, Li W and Pei Y Z 2021 *Sci. Adv.* **7** eabf2738
[18] Lewis J E 1969 *Phys. Status Solidi* **35** 737
[19] Damon D H, Lubell M S and Mazelsky R 1967 *J. Phys. Chem. Solids* **28** 520
[20] Edwards A H, Pineda A C, Schultz P A, Martin M G, Thompson A P, Hjalmarson H P and Umrigar C J 2006 *Phys. Rev. B* **73** 45210
[21] Perumal S, Bellare P, Shenoy U S, Waghmare U V and Biswas K 2017 *Chem. Mater.* **29** 10426
[22] Perumal S, Roychowdhury S, Negi D S, Datta R and Biswas K 2015 *Chem. Mater.* **27** 7171
[23] Li J, Zhang X, Lin S, Chen Z and Pei Y 2017 *Chem. Mater.* **29** 605
[24] Li J, Chen Z, Zhang X, Yu H, Wu Z, Xie H, Chen Y and Pei Y 2017 *Adv. Sci.* **4** 1700341
[25] Zheng Z, Su X, Deng R, Stoumpos C, Xie H, Liu W, Yan Y, Hao S, Uher C, Wolverton C, Kanatzidis M G and Tang X 2018 *J. Am. Chem. Soc.* **140** 2673
[26] Hong M, Wang Y, Liu W, Matsumura S, Wang H, Zou J and Chen Z G 2018 *Adv. Energy Mater.* **8** 1801837
[27] Hong M, Wang Y, Feng T, Sun Q, Xu S, Matsumura S, Pantelides S T, Zou J and Chen Z G 2019 *J. Am. Chem. Soc.* **141** 1742
[28] Sun P, Kumar K R, Lyu M, Wang Z, Xiang J and Zhang W 2021 *Innovation* **2** 100101
[29] Ciucivara A, Sahu B R and Kleinman L 2007 *Phys. Rev. B* **75** 241201

[30] Wang R F, Li S, Xue W H, Chen C, Wang Y M, Liu X J and Zhang Q 2021 *Rare Met.* **40** 40
[31] Nielsen M D, Ozolins V and Heremans J P 2013 *Energy Environ. Sci.* **6** 570
[32] Xu X, Xie L, Lou Q, Wu D and He J 2018 *Adv. Sci.* **5** 1801514
[33] Chattopadhyay T, Boucherle J X and VonSchnering H G 1987 *J. Phys. C: Solid State Phys.* **20** 1431
[34] Lee H S, Kim B S, Cho C W, Oh M W, Min B K, Park S D and Lee H W 2015 *Acta Mater.* **91** 83
[35] Bu Z, Chen Z, Zhang X, Lin S, Mao J, Li W, Chen Y and Pei Y 2020 *Mater. Today Phys.* **15** 100260
[36] Cao J, Chien S W, Tan X Y, Tan C K I, Zhu Q, Wu J, Wang X, Zhao Y, Yang L, Yan Q, Liu H, Xu J and Suwardi A 2021 *ChemNanoMat* **7** 476
[37] Askarpour V and Maassen J 2019 *Phys. Rev. B* **100** 75201
[38] Gibbs Z M, Ricci F, Li G, Zhu H, Persson K, Ceder G, Hautier G, Jain A and Snyder G J 2017 *npj Comput. Mater.* **3** 8
[39] Samanta M, Ghosh T, Arora R, Waghmare U V and Biswas K 2019 *J. Am. Chem. Soc.* **141** 19505
[40] Liu Z, Sato N, Guo Q, Gao W and Mori T 2020 *NPG Asia Mater.* **12** 66
[41] Robertson J 1983 *Phys. Rev. B* **28** 4671
[42] Van de Walle C G and Neugebauer J 2004 *J. Appl. Phys.* **95** 3851
[43] Kresse G and Furthmüller J 1996 *Phys. Rev. B* **54** 11169
[44] Perdew J P, Burke K and Ernzerhof M 1996 *Phys. Rev. Lett.* **77** 3865
[45] Huo H, Wang Y, Xi L, Yang J and Zhang W 2021 *J. Mater. Chem. C* **9** 5765
[46] Bu Z, Li W, Li J, Zhang X, Mao J, Chen Y and Pei Y 2019 *Mater. Today Phys.* **9** 100096
[47] Xie L, Chen Y, Liu R, Song E, Xing T, Deng T, Song Q, Liu J, Zheng R, Gao X, Bai S and Chen L 2020 *Nano Energy* **68** 104347
[48] Yue L, Fang T, Zheng S, Cui W, Wu Y, Chang S, Wang L, Bai P and Zhao H 2019 *ACS Appl. Energy Mater.* **2** 2596
[49] Zhang X, Li J, Wang X, Chen Z, Mao J, Chen Y and Pei Y 2018 *J. Am. Chem. Soc.* **140** 15883
[50] Snyder G J, Snyder A H, Wood M, Gurunathan R, Snyder B H and Niu C 2020 *Adv. Mater.* **32** 2001537
[51] Ren Q, Fu C, Qiu Q, Dai S, Liu Z, Masuda T, Asai S, Hagihala M, Lee S, Torri S, Kamiyama T, He L, Tong X, Felser C, Singh D J, Zhu T, Yang J and Ma J 2020 *Nat. Commun.* **11** 3142
[52] Goldsmid H J and Sharp J W 1999 *J. Electron. Mater.* **28** 869
[53] Cahill D G, Watson S K and Pohl R O 1992 *Phys. Rev. B* **46** 6131